Real-time exciton dynamics with time-dependent density-functional theory

Jiuyu Sun,[1,2] Cheng-Wei Lee,[3] Alina Kononov,[4] André Schleife,[3,5,6] and Carsten A. Ullrich[1]

[1]*Department of Physics and Astronomy, University of Missouri, Columbia, Missouri 65211, USA*
[2]*Max Planck Institute for the Structure and Dynamics of Matter, 22761 Hamburg, Germany*
[3]*Department of Materials Science and Engineering,*
University of Illinois at Urbana-Champaign, Urbana, Illinois 61801, USA
[4]*Department of Physics, University of Illinois at Urbana-Champaign, Urbana, Illinois 61801, USA*
[5]*Materials Research Laboratory, University of Illinois at Urbana-Champaign, Urbana, Illinois 61801, USA*
[6]*National Center for Supercomputing Applications,*
University of Illinois at Urbana-Champaign, Urbana, Illinois 61801, USA
(Dated: July 13, 2021)

Linear-response time-dependent density-functional theory (TDDFT) can describe excitonic features in the optical spectra of insulators and semiconductors, using exchange-correlation (xc) kernels behaving as $-1/k^2$ to leading order. We show how excitons can be modeled in real-time TDDFT, using an xc vector potential constructed from approximate, long-range corrected xc kernels. We demonstrate for various materials that this real-time approach is consistent with frequency-dependent linear response, gives access to femtosecond exciton dynamics following short-pulse excitations, and can be extended with some caution into the nonlinear regime.

Introduction.—Optical spectra of electronic systems can be calculated from first principles in two alternative ways: Using frequency-dependent linear response (LR) theory, or via real-time (RT) propagation of the electronic wave function following a short initial excitation and then Fourier transforming the induced current fluctuations [1, 2]. The RT description has several benefits: for large systems it becomes computationally advantageous over LR [3]; while both theories allow coupling to nuclear dynamics, RT gives easy access to ultrafast (as/fs), transient, and nonlinear processes [4–6].

To describe the dynamics of interacting electrons, time-dependent density-functional theory (TDDFT) is an accurate yet computationally efficient choice [7–9]. Here, our interest is in RT electron dynamics of optically excited periodic solids with a band gap. RT-TDDFT for solids has a long history [10, 11]: Besides the calculation of optical spectra, it has been used to simulate two-photon absorption and ultrafast dielectric response [12–15], coherent phonons and stimulated Raman scattering [16], ultrafast laser-induced metal-insulator transitions [17], nonlinear optical response and high-order harmonic generation [18–20], photoelectron spectroscopy [21], electronic stopping power [22, 23], ultrafast demagnetization and magnons [24, 25], as well as core excitations [26–28].

In Refs. [10–26], (semi)local exchange-correlation (xc) functionals were used, i.e., the adiabatic local-density approximation (ALDA) or generalized gradient approximations (GGA). This causes a serious problem for semiconductors and insulators: (semi)local xc approximations cannot describe excitons [1, 29], and therefore produce physically wrong optical absorption spectra. Excitonic features can be captured in RT using hybrid functionals [2, 27, 28] or the Bethe-Salpeter equation (BSE) [30]. However, these methods are computationally much more demanding than pure xc density functionals.

The main purpose of this paper is to provide proof of concept that RT-TDDFT is capable of describing excitonic effects. The idea is to generalize the so-called long-range corrected (LRC) xc kernels from LR-TDDFT [31–36] into the RT regime; the result is an xc vector potential that accounts for the long-range screened electron-hole interaction that causes the formation of excitons. We implement this approach in Qb@ll [37–39], and demonstrate that it produces optical spectra consistent with LR. We then present applications illustrating the capabilities and limitations of this approach, including ultrafast and non-linear effects.

Theoretical background.—In LR-TDDFT, interacting electronic systems respond to the sum of external perturbation plus linearized Hartree and xc potentials. The latter are determined by the Hartree kernel $f_{\mathrm{H}}(\mathbf{r}, \mathbf{r}') = 1/|\mathbf{r} - \mathbf{r}'|$ and the xc kernel $f_{\mathrm{xc}}(\mathbf{r}, \mathbf{r}', \omega)$; the xc kernel—a functional of the ground-state density $n_{\mathrm{gs}}(\mathbf{r})$—has to be approximated in practice. This formalism is widely used to calculate excitation energies and optical spectra [8, 9].

In a periodic solid, optical absorption is defined with respect to the total macroscopic classical perturbation, including the induced field [1, 40]. LR-TDDFT accounts for this via a modified Hartree kernel, which in reciprocal space is given by $f_{\mathrm{H},\mathbf{G}\mathbf{G}'}^{\mathrm{mod}}(\mathbf{k}) = \frac{4\pi}{|\mathbf{k}+\mathbf{G}|^2} \delta_{\mathbf{G},\mathbf{G}'}(1 - \delta_{\mathbf{G},\mathbf{0}})$ [36]. Here, $\mathbf{G}, \mathbf{G}'$ are reciprocal lattice vectors, and $\mathbf{k}$ is a wavevector in the first Brillouin zone. The modification thus consists in setting the head of the Hartree kernel (where $\mathbf{G} = \mathbf{G}' = 0$) to zero.

To describe optical excitations, we need the xc kernel $f_{\mathrm{xc},\mathbf{G}\mathbf{G}'}(\mathbf{k}, \omega)$ in the limit $\mathbf{k} \to 0$. It is a known analytic property that in this limit the head of the xc kernel diverges as k^{-2}, the wing elements ($\mathbf{G} = 0$, $\mathbf{G}'$ finite and vice versa) diverge as k^{-1}, and the body elements ($\mathbf{G}, \mathbf{G}'$ finite) approach a constant [41, 42]. In three-dimensional bulk solids, the k^{-2} behavior of the head of $f_{\mathrm{xc},\mathbf{G}\mathbf{G}'}(\mathbf{k}, \omega)$

is the dominant effect causing the formation of excitons [1]. Several approximations which capture this behavior have been proposed [31–36], most of them independent of ω (adiabatic approximation). Here, we consider the simplest of these, the LRC xc kernel [31, 34]:

$$f_{\text{xc},\mathbf{GG}'}^{\text{LRC}}(\mathbf{k}) = -\frac{\alpha}{|\mathbf{k}+\mathbf{G}|^2}\,\delta_{\mathbf{G},\mathbf{G}'}\,, \qquad (1)$$

where α is, in principle, a functional of n_{gs}, but here we treat it as a material-dependent empirical parameter. With a suitable choice of α, the LRC kernel can reproduce the main features in the optical absorption spectra of insulators and semiconductors, including strongly bound and continuum excitons [36, 43]. In the following, we limit ourselves to the head-only LRC kernel, i.e., we set $f_{\text{xc},\mathbf{GG}'}^{\text{LRC}}(\mathbf{k}) = 0$ unless $\mathbf{G} = \mathbf{G}' = \mathbf{0}$.

The ALDA lacks the long-range ($\mathbf{k} \to 0$) behavior required for an excitonic xc kernel; however, it does contribute short-range local-field effects ($\mathbf{G}, \mathbf{G}'$ nonzero), which can impact the spectral shape. We will take advantage of this by defining a combined (LRC$_+$) xc kernel,

$$f_{\text{xc}}^{\text{LRC}_+} = f_{\text{xc}}^{\text{LRC}} + \beta f_{\text{xc}}^{\text{ALDA}}, \qquad (2)$$

where β is an adjustable parameter which gives us some flexibility to improve LRC spectral features, if needed.

The xc kernel is defined as the functional derivative of the time-dependent xc potential $v_{\text{xc}}(\mathbf{r},t)$. In the ALDA, this becomes $f_{\text{xc}}^{\text{ALDA}}(\mathbf{r},\mathbf{r}') = \delta v_{\text{xc}}^{\text{LDA}}[n](\mathbf{r})/\delta n(\mathbf{r}')|_{n_{\text{gs}}(\mathbf{r})}$. However, for excitonic xc kernels such as the so-called bootstrap kernel [44], no comparable relation exists: most excitonic xc kernels currently in use [35, 36] are not defined as the functional derivative of an xc potential. It is thus not immediately obvious how to go from LR- to RT-TDDFT for this class of functionals; however, for the simple LRC xc kernel (1) it is relatively straightforward, as we shall now discuss.

Consider a solid which is initially in the ground state associated with a periodic lattice potential $v(\mathbf{r})$. We assume that the band structure has been calculated using LDA or a GGA (which may underestimate the band gap, but this is not our major concern here). At time $t = 0$, a time-dependent perturbation is switched on, in the form of a scalar potential $v'(\mathbf{r},t)$ and/or a vector potential $\mathbf{A}'(\mathbf{r},t)$. Formally, this requires the framework of time-dependent current-DFT [8], featuring time-dependent xc scalar and vector potentials $v_{\text{xc}}(\mathbf{r},t)$ and $\mathbf{A}_{\text{xc}}(\mathbf{r},t)$, and the system evolves under the time-dependent Kohn-Sham equation in the velocity gauge [26]:

$$i\frac{\partial}{\partial t}\varphi_j(\mathbf{r},t) = \left[\frac{1}{2}\left(\frac{\nabla}{i} + \mathbf{A}'(\mathbf{r},t) + \mathbf{A}_{\text{xc}}(\mathbf{r},t)\right)^2\right.$$
$$\left. + v(\mathbf{r}) + v'(\mathbf{r},t) + v_{\text{H}}(\mathbf{r},t) + v_{\text{xc}}(\mathbf{r},t)\right]\varphi_j(\mathbf{r},t)\,. \quad (3)$$

The time-dependent density can be written as $n(\mathbf{r},t) = n_{\text{gs}}(\mathbf{r}) + \delta n(\mathbf{r},t)$, where the density response $\delta n(\mathbf{r},t)$ is not necessarily small compared to the lattice-periodic $n_{\text{gs}}(\mathbf{r})$. Recalling that the optical response requires removing the long-range ($\mathbf{G} = 0$) part of the classical Coulomb interaction, the time-dependent Hartree potential takes the form $v_{\text{H}}(\mathbf{r},t) = v_{\text{H}}[n_{\text{gs}}](\mathbf{r}) + v_{\text{H}}^{\text{mod}}[\delta n](\mathbf{r},t)$, using the modified Hartree kernel discussed above.

Next, we consider the time-dependent xc effects. The ALDA xc potential $v_{\text{xc}}^{\text{ALDA}}[n](\mathbf{r},t)$ matches the ground-state LDA, but does not produce excitonic binding. To generate excitons we include additional, purely dynamical xc effects based on the LRC kernel (1), see Supplemental Material (SM) [45] for details. The resulting LRC xc scalar potential [46] is $v_{\text{xc}}^{\text{LRC}}(\mathbf{r},t) = \int d\mathbf{r}' f_{\text{xc}}^{\text{LRC}}(\mathbf{r},\mathbf{r}')\delta n(\mathbf{r}',t)$ in real space and $v_{\text{xc},\mathbf{G}}^{\text{LRC}}(t) = -(\alpha/|\mathbf{G}|^2)\delta n_{\mathbf{G}}(t)$ in reciprocal space, making use of the lattice periodicity of the density response. However, the long-range ($\mathbf{G} = 0$) component of $v_{\text{xc},\mathbf{G}}^{\text{LRC}}(t)$ is ill-defined, in spite of the fact that $\delta n_{\mathbf{0}}(t) = 0$ due to charge conservation. This problem can be avoided by transforming into an xc vector potential [47]. In real space, we obtain

$$\mathbf{A}_{\text{xc}}^{\text{LRC}}(\mathbf{r},t) = -\frac{\alpha}{4\pi}\int_0^t dt'\int_0^{t'}dt''\nabla\int d\mathbf{r}'\frac{\nabla'\cdot\mathbf{j}(\mathbf{r}',t'')}{|\mathbf{r}-\mathbf{r}'|}\,, \quad (4)$$

where the current density $\mathbf{j}(\mathbf{r},t)$ enters via the continuity equation $\nabla\cdot\mathbf{j}(\mathbf{r},t) = -\partial n(\mathbf{r},t)/\partial t$, and the scalar and vector potentials are connected through the gauge relation $\partial\mathbf{A}_{\text{xc}}^{\text{LRC}}(\mathbf{r},t)/\partial t = -\nabla v_{\text{xc}}^{\text{LRC}}(\mathbf{r},t)$. Since the head of the LRC xc kernel (1) is dominant for optical excitations, we only include the macroscopic current density $\mathbf{j_0}$ in the LRC vector potential [48]. Thus, we end up with

$$\mathbf{A}_{\text{xc},\mathbf{G}}^{\text{LRC}}(t) = \alpha\int_0^t dt'\int_0^{t'}dt''\mathbf{j}_{\mathbf{G}}(t'')\delta_{\mathbf{G},\mathbf{0}}\,, \quad (5)$$

which can also be written as a differential equation: $d^2\mathbf{A}_{\text{xc},\mathbf{0}}^{\text{LRC}}(t)/dt^2 = \alpha\mathbf{j_0}(t)$. The total current density is the sum of the paramagnetic current density $\mathbf{j}_p = (2i)^{-1}\sum_j\varphi_j^*(\mathbf{r},t)\nabla\varphi_j(\mathbf{r},t) + c.c.$ and a diamagnetic contribution featuring the vector potentials. Thus, the macroscopic total current density is

$$\mathbf{j_0}(t) = \mathbf{j}_{p,\mathbf{0}}(t) + (\mathbf{A}_{\mathbf{0}}'(t) + \mathbf{A}_{\text{xc},\mathbf{0}}^{\text{LRC}}(t))n_{\text{gs},\mathbf{0}}\,, \quad (6)$$

where $n_{\text{gs},\mathbf{0}}$ is the average ground-state density. An RT-TDDFT formalism that is consistent with the LRC$_+$ kernel (2) is obtained by using $\mathbf{A}_{\text{xc}}^{\text{LRC}}(t)$ and a β-scaled scalar ALDA xc potential, $v_{\text{xc},\beta}^{\text{ALDA}}(t)$, in Eq. (3). The β-scaling only affects the response part of $v_{\text{xc}}^{\text{ALDA}}(t)$ associated with $\delta n(t)$; see SM [45] for more details. As before, we shall refer to this combined RT-TDDFT approach as LRC$_+$.

Results and discussion.—In the following, we present results for Si, LiF, CsGeCl$_3$, and an H$_2$ chain. The RT-TDDFT calculations were done with Qb@ll [37–39], and we compare with LR-TDDFT and BSE calculations using Yambo [49] and Quantum Espresso [50] (for computational details see SM [45]).
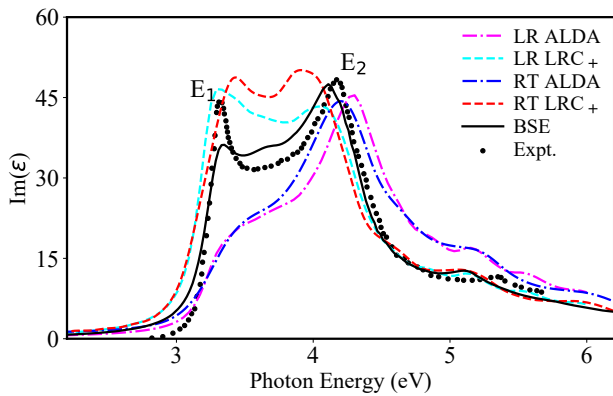
FIG. 1. Optical spectra $\text{Im}(\varepsilon)$ of Si, obtained by LR- and RT-TDDFT, compared with BSE and experiment [51]. The calculated spectra are scissor shifted for the onset to line up with experiment (see SM for details [45]).

FIG. 2. Response of Si to 10 fs laser pulses (frequency 1.6 eV, polarized along z) with peak intensities 10^7 W/cm^2 (top) and 10^{11} W/cm^2 (bottom), comparing ALDA and LRC$_+$ within RT-TDDFT. (a) Induced current density $j_z(t)$. (b) Dipole power spectrum $|P(\omega)|^2$.

We begin with Si, to verify the consistency between RT- and LR-TDDFT. The LRC kernel (1) was originally proposed to reproduce the optical spectrum of Si using $\alpha = 0.2$ [31]. Thus, we compare $f_{\text{xc}}^{\text{ALDA}}$ and $f_{\text{xc}}^{\text{LRC}_+}$ (with $\beta = 1$) in LR, and solve Eq. (3) using the corresponding ALDA and LRC$_+$ potentials. Starting from the Kohn-Sham ground state, the system is excited by a delta-peaked uniform electric field along the z-direction, which leads to a constant $\mathbf{A}'$ switched on at $t = 0$ (see SM [45]). The dielectric function $\varepsilon(\omega)$ is obtained from the induced current fluctuations, following Yabana *et al.* [11, 13].

Figure 1 shows the imaginary part of the dielectric function $\text{Im}(\varepsilon)$ of Si obtained by different approaches, as well as experimental data. The LR-ALDA and RT-ALDA spectra are very similar: both seriously underestimate the first absorption peak E_1 around 3.2 eV [1, 31]. In BSE, the E_1 peak is strongly enhanced compared to ALDA, though still somewhat lower than experiment. A better agreement between BSE and experiment could be achieved with a much denser $\mathbf{k}$-grid or other improvements [52, 53], but this is not the main focus of our study.

It is evident from Fig. 1 that LRC dramatically improves the ALDA spectrum: both LR- and RT-LRC$_+$ curves show double-peak structures, with an E_1 peak height comparable to E_2, which agrees better with experiment than BSE. Both LRC$_+$ spectra also correct the overestimation beyond 4.5 eV by ALDA. The differences between the LR and RT spectra are mainly due to the different $\mathbf{k}$-point sampling used in Qb@ll and Yambo, as discussed in the SM [45]. Aside from these minor technical details, our results clearly show that excitonic effects in materials with weakly bound excitons, such as Si, can be well described with RT-TDDFT using LRC$_+$.

RT-TDDFT is not limited to weak perturbations, but allows us to explore ultrafast and nonlinear electron dynamics. The LRC$_+$ parameters can be assumed to remain unc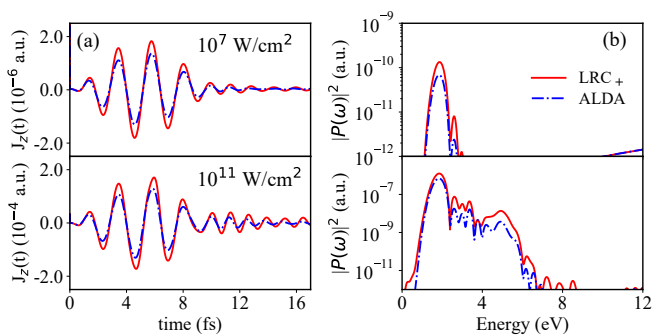hanged as long as we do not stray too far from the linear regime. Instead of a delta-peaked uniform electric field, we apply short laser pulses polarized along the z-axis with frequency 1.6 eV, $\sin^2$ envelope, and 10 fs pulse duration. We consider weak and strong pulses with peak intensity 10^7 and 10^{11} W/cm^2, respectively. Figure 2a shows that the z-component of the total macroscopic current density j_z^{tot} propagated with LRC$_+$ has a larger amplitude than with ALDA. There are two reasons for the enhanced current response: (i) LRC drastically increases the oscillator strength at the absorption edge (see Fig. 1), leading to a stronger coupling to the laser; (ii) the diamagnetic contribution to the total current, Eq. (6), may be enhanced by the LRC xc vector potential. While the system is driven by the laser, the induced currents scale with the square root of the intensity; the remaining current oscillations after the end of the pulse are more pronounced at 10^{11} W/cm^2, indicating nonlinearity.

The associated dipole power spectra $|P(\omega)|^2$ (see SM [45]) are shown in Fig. 2b. At low laser intensity, ALDA and LRC$_+$ produce very similar spectra, with a dominant peak at 1.6 eV and a smooth drop-off at higher frequencies. Nonlinear effects become significant at 10^{11} W/cm^2 pulse intensity: the ALDA and LRC$_+$ spectra both extend towards higher frequencies, and there is a broad peak around 5 eV (the 3rd harmonic of the pulse). Overall, LRC$_+$ gives a more pronounced nonlinear response than ALDA, which is in agreement with a study using time-dependent polarization-DFT [54].

Next, we explore strongly bound excitons in insulators. We begin with a chain of H$_2$ molecules with a finite gap (see SM [45]). Figure 3a shows that BSE yields a pronounced excitonic peak around 3.6 eV which the ALDA fails to reproduce. LR-TDDFT with the LRC kernel improves the spectra: for $\alpha = 18.0$ we obtain an excitonic peak of similar height and shape as the BSE, but at a higher energy. An even larger α would put the peak at the right position, but with too much oscillator strength, consistent with earlier studies of the LRC kernel [35].

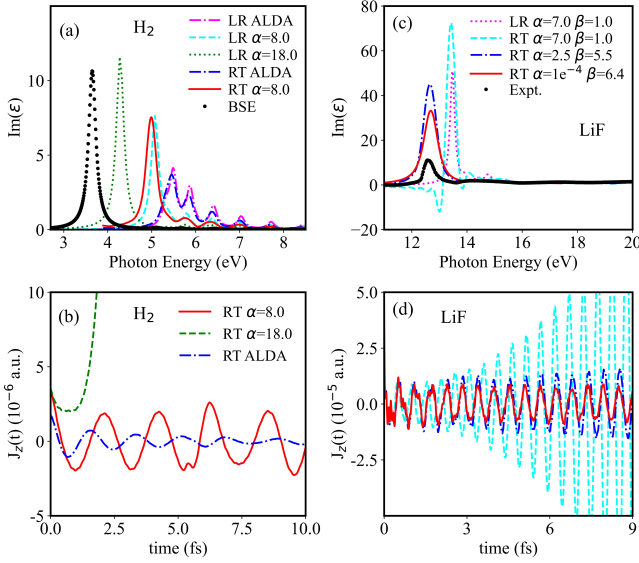FIG. 3. Strongly bound excitons in an H_2 chain (left) and LiF (right). (a) Im(ε) from BSE and TDDFT; (b) macroscopic current density from RT ALDA and LRC with $\alpha = 8$ and 18; (c) Im(ε) from LRC$_+$ in LR and RT, with α and β as indicated, versus experiment [55]; (d) macroscopic current density from the same three RT-LRC$_+$ as in (c).

Note that we here set $\beta = 0$ to avoid numerical difficulties in Yambo when combining LRC with ALDA, due to an enhanced sensitivity to local-field effects in 1D.

For $\alpha = 8.0$, LR- and RT-TDDFT of the H_2 chain are in close agreement. However, we found that at $\alpha = 18.0$ the RT calculation failed. Figure 3b shows that at $\alpha = 8.0$ the induced current is comparable to the ALDA current, but at $\alpha = 18.0$ the current rapidly diverges.

To investigate this further, we now consider LiF. The experimental optical spectrum (Fig. 3c) features a prominent excitonic peak around 12.6 eV. LR-TDDFT with LRC$_+$ using $\alpha = 7$ and $\beta = 1$ gives a blue-shifted exciton at 13.5 eV; a larger value of α could be used to shift the exciton down to the correct position, but with much exaggerated peak height [35].

RT-TDDFT using LRC$_+$ with the same parameters ($\alpha = 7, \beta = 1$) appears to be developing an instability, as indicated by the current density in Fig. 3d, which keeps increasing after 2 fs. The resulting LiF optical spectrum (cyan curve in Fig. 3c) is peaked at 13.5 eV but has a distorted shape. The current response can be stabilized by decreasing α, and the excitonic peak can be shifted to the correct position by increasing β, as illustrated in Figs. 3c and d. Indeed, comparing ($\alpha = 2.5, \beta = 5.5$) and ($\alpha = 10^{-4}, \beta = 6.4$) we find that the latter produces the best agreement with experiment. In this case, the excitonic interactions arise from the up-scaled ALDA local-field effects, like in the so-called contact exciton [56, 57]. This scaling approach is effective because of the tightly bound excitons in LiF; local-field effects are much less important
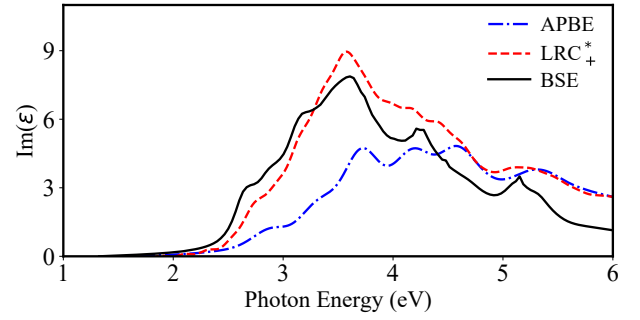

FIG. 4. Optical spectra of CsGeCl$_3$ obtained by BSE and RT-TDDFT using APBE and LRC$_+^*$.

for systems with weakly bound, delocalized excitons.

What is the reason for the LRC instabilities? The zero-force theorem of TDDFT [8] states that the total force due to xc scalar and vector potentials must vanish:

$$0 = \int d\mathbf{r} \Big[- n(\mathbf{r},t)\nabla v_{xc}(\mathbf{r},t) - n(\mathbf{r},t)\frac{\partial}{\partial t}\mathbf{A}_{xc}(\mathbf{r},t)$$
$$+ \mathbf{j}(\mathbf{r},t) \times \nabla \times \mathbf{A}_{xc}(\mathbf{r},t) \Big]. \tag{7}$$

The ALDA satisfies the zero-force theorem. $\mathbf{A}_{xc}^{LRC}$ is strictly longitudinal, so the last term in Eq. (7) vanishes. From Eq. (5), the second term in Eq. (7) becomes $-\alpha N \int_0^t dt' \mathbf{j_0}(t')$. Thus, LRC produces a macroscopic xc force, which can cause instabilities in the current oscillations for strongly bound excitons due to their large oscillator strength, as seen in H_2 and LiF. This violation of the zero-force theorem is also present in f_{xc}^{LRC}, but still allows one to obtain good optical spectra via LR-TDDFT, albeit with an exaggerated peak height for strongly bound excitons [35]. Instabilities may show up during RT propagation, even if initiated with a weak perturbation, due to self-amplification of small fluctuations [58].

As a final illustration of RT-TDDFT, we now return to a system with weakly bound excitons and consider a more complex material, the perovskite CsGeCl$_3$. To our knowledge, no experimental optical spectra of this material are available. We adopt a cubic phase of $Pm\bar{3}m$, where a Ge atom substitutes the Pb atom in the popular CsPbCl$_3$, which allows us to neglect spin-orbit coupling.

Figure 4 shows the optical spectrum of CsGeCl$_3$, calculated using G_0W_0+BSE. The G_0W_0 band gap is 2.96 eV; the BSE spectrum displays a relatively weak shoulder around 2.6 eV, and a dominant continuum exciton peak at 3.5 eV. We compare with RT-TDDFT spectra obtained using adiabatic PBE (APBE) [59] and APBE+LRC (LRC$_+^*$) using $\alpha = 1.1$. It is found that the APBE and LRC$_+^*$ spectra are almost on top of each other beyond 4.6 eV, and are both very similar to BSE in this range. At lower energies, APBE, a semilocal functional, significantly underestimates Im(ε); this is similar to the failure of ALDA for Si. On the other hand, the

overall spectral shape of LRC^*_+ is very close to BSE, even reproducing the weak shoulder around 2.8 eV. The associated induced current densities (see SM [45]) are well behaved and stable, and no β-scaling is needed.

Conclusions.—In this paper, we have demonstrated that TDDFT can describe excitons in periodic solids by propagating the time-dependent Kohn-Sham equation following an initial short-pulse excitation. LR-TDDFT has long been known to be capable of producing excitonic optical spectra using xc kernels with the appropriate long-range behavior. Here, we have shown how the simplest of these, the LRC kernel, can be converted into an xc vector potential featuring the macroscopic current density and an adjustable parameter, α; the additional computational cost beyond the ALDA is negligible.

Applications to Si, H_2 chain, LiF, and $CsGeCl_3$ show that LR- and RT-TDDFT are consistent in the sense that they produce essentially the same optical spectra in the weakly perturbed regime, but RT-TDDFT can be applied beyond the linear regime to describe ultrafast and nonlinear exciton dynamics. However, the LRC xc functional has its limitations: in materials with strongly bound excitons, it can lead to instabilities in the induced currents, which is a consequence of violating the zero-force theorem. In materials with weakly bound or continuum excitons, no such problems occurred.

This study opens up multiple paths towards TDDFT studies of exciton dynamics in bulk materials and nanostructures. An important task for future research will be to find parameter-free xc functionals for RT-TDDFT beyond LRC, or adjust LRC to satisfy the zero-force theorem. Our RT-TDDFT approach can be combined with recently developed visualization methods for exciton wave functions [46], and it is possible to study exciton relaxation effects by coupling to nuclear dynamics at the Ehrenfest level [23].

[1] G. Onida, L. Reining, and A. Rubio, Electronic excitations: density-functional versus many-body Green's-function approaches, Rev. Mod. Phys. **74**, 601 (2002).

[2] T. Sander and G. Kresse, Macroscopic dielectric function within time-dependent density functional theory—real time evolution versus the Casida approach, J. Chem. Phys. **146**, 064110 (2017).

[3] C. Müller, M. Sharma, and M. Sierka, Real-time time-dependent density functional theory using density fitting and the continuous fast multipole method, J. Comp. Chem. **41**, 2573 (2020).

[4] C. A. Rozzi, S. M. Falke, N. Spallanzani, A. Rubio, E. Molinari, D. Brida, M. Maiuri, G. Cerullo, H. Schramm, J. Christoffers, and C. Lienau, Quantum coherence controls the charge separation in a prototypical artificial light-harvesting system, Nature Commun. **4**, 1602 (2017).

[5] S. A. Sato, H. Hübener, U. De Giovannini, and A. Rubio, Ab initio simulation of attosecond transient absorption spectroscopy in two-dimensional materials, Appl. Sci. **8**, 1777 (2018).

[6] X. Li, N. Govind, C. Isborn, A. E. DePrince III, and K. Lopata, Real-time time-dependent electronic structure theory, Chem. Rev. **120**, 9951 (2020).

[7] E. Runge and E. K. U. Gross, Density-functional theory for time-dependent systems, Phys. Rev. Lett. **52**, 997 (1984).

[8] C. A. Ullrich, *Time-dependent density-functional theory: concepts and applications* (Oxford University Press, Oxford, 2012).

[9] M. E. Casida and M. Huix-Rotllant, Progress in time-dependent density-functional theory, Annu. Rev. Phys. Chem. **63**, 287–323 (2012).

[10] G. F. Bertsch, J.-I. Iwata, A. Rubio, and K. Yabana, Real-space, real-time method for the dielectric function, Phys. Rev. B **62**, 7998 (2000).

[11] K. Yabana, T. Nakatsukasa, J.-I. Iwata, and G. F. Bertsch, Real-time, real-space implementation of the linear response time-dependent density-functional theory, phys. stat. sol. (b) **243**, 1121 (2006).

[12] T. Otobe, M. Yamagiwa, J.-I. Iwata, K. Yabana, T. Nakatsukasa, and G. F. Bertsch, First-principles electron dynamics simulation for optical breakdown of dielectrics under an intense laser field, Phys. Rev. B **77**, 165104 (2008).

[13] K. Yabana, T. Sugiyama, Y. Shinohara, T. Otobe, and G. F. Bertsch, Time-dependent density functional theory for strong electromagnetic fields in crystalline solids, Phys. Rev. B **85**, 045134 (2012).

[14] G. Su, F. Wang, L. Jiang, X. Zhang, X. Su, L. Qu, and Y. Lu, Ultrafast response of dielectric properties of monolayer phosphorene to femtosecond laser, J. Chem. Phys. **121**, 173105 (2017).

[15] X. Zhang, F. Wang, L. Jiang, and Y. Yao, Manipulation of the dielectric properties of diamond by an ultrashort laser pulse, Phys. Rev. B **95**, 184301 (2017).

[16] A. Yamada and K. Yabana, Multiscale time-dependent density functional theory for a unified description of ultrafast dynamics: Pulsed light, electron, and lattice motions in crystalline solids, Phys. Rev. B **99**, 245103 (2019).

[17] G. Wachter, C. Lemell, J. Burgdörfer, S. A. Sato, X.-M. Tong, and K. Yabana, Ab initio simulation of electrical currents induced by ultrafast laser excitation of dielectric materials, Phys. Rev. Lett. **113**, 087401 (2014).

[18] V. A. Goncharov, Nonlinear optical response in solids from time-dependent density-functional theory simulations, J. Chem. Phys. **139**, 084104 (2013).

[19] N. Tancogne-Dejean, O. D. Mücke, F. X. Kärtner, and

A. Rubio, Impact of the electronic band structure in high-harmonic generation spectra of solids, Phys. Rev. Lett. **118**, 087403 (2017).

[20] N. Tancogne-Dejean, O. D. Mücke, F. X. Kärtner, and A. Rubio, Ellipticity dependence of high-harmonic generation in solids originating from coupled intraband and interband dynamics, Nature Commun. **8**, 745 (2017).

[21] U. De Giovannini, H. Hübener, and A. Rubio, A first-principles time-dependent density functional theory framework for spin and time-resolved angular-resolved photoelectron spectroscopy in periodic systems, J. Chem. Theory Comput. **13**, 265 (2017).

[22] J. M. Pruneda, D. Sánchez-Portal, A. Arnau, J. I. Juaristi, and E. Artacho, Electronic stopping power in LiF from first principles, Phys. Rev. Lett. **99**, 235501 (2007).

[23] A. Schleife, Y. Kanai, and A. A. Correa, Accurate atomistic first-principles calculations of electronic stopping, Phys. Rev. B **91**, 014306 (2015).

[24] K. Krieger, J. K. Dewhurst, P. Elliott, S. Sharma, and E. K. U. Gross, Laser-induced demagnetization at ultrashort time scales: Predictions of TDDFT, J. Chem. Theor. Comput. **11**, 4870 (2015).

[25] N. Tancogne-Dejean, F. D. Eich, and A. Rubio, Time-dependent magnons from first principles, J. Chem. Tneory Comput. **16**, 1007 (2020).

[26] C. D. Pemmaraju, F. D. Vila, J. J. Kas, S. A. Sato, J. J. Rehr, and K. Yabana, Velocity-gauge real-time TDDFT within a numerical atomic orbital basis set, Comput. Phys. Commun. **226**, 30 (2018).

[27] C. D. Pemmaraju, Valence and core excitons in solids from velocity-gauge real-time TDDFT with range-separated hybrid functionals: An LCAO approach, Comput. Condensed Matter **16**, e00348 (2018).

[28] C. D. Pemmaraju, Simulation of attosecond transient soft x-ray absorption in solids using generalized Kohn–Sham real-time time-dependent density functional theory, New J. Phys. **22**, 083063 (2020).

[29] C. A. Ullrich and Z.-H. Yang, Excitons in time-dependent density-functional theory, in *Density-Functional Methods for Excited States*, Topics in Current Chemistry, Vol. 368, edited by N. Ferré, M. Filatov, and M. Huix-Rotllant (Springer, Berlin, 2015) p. 185.

[30] C. Attaccalite, M. Grüning, and A. Marini, Real-time approach to the optical properties of solids and nanostructures: Time-dependent Bethe-Salpeter equation, Phys. Rev. B **84**, 245110 (2011).

[31] L. Reining, V. Olevano, A. Rubio, and G. Onida, Excitonic effects in solids described by time-dependent density-functional theory, Phys. Rev. Lett. **88**, 066404 (2002).

[32] F. Sottile, V. Olevano, and L. Reining, Parameter-free calculation of response functions in time-dependent density-functional theory, Phys. Rev. Lett. **91**, 056402 (2003).

[33] A. Marini, R. Del Sole, and A. Rubio, Bound excitons in time-dependent density-functional theory: optical and energy-loss spectra, Phys. Rev. Lett. **91**, 256402 (2003).

[34] S. Botti, F. Sottile, N. Vast, V. Olevano, L. Reining, H.-C. Weissker, A. Rubio, G. Onida, R. Del Sole, and R. W. Godby, Long-range contribution to the exchange-correlation kernel of time-dependent density functional theory, Phys. Rev. B **69**, 155112 (2004).

[35] Y.-M. Byun and C. A. Ullrich, Assessment of long-range-corrected exchange-correlation kernels for solids: Accu-

rate exciton binding energies via an empirically scaled bootstrap kernel, Phys. Rev. B **95**, 205136 (2017).

[36] Y.-M. Byun, J. Sun, and C. A. Ullrich, Time-dependent density-functional theory for periodic solids: assessment of excitonic exchange-correlation kernels, Electron. Struct. **2**, 023002 (2020).

[37] E. W. Draeger and F. Gygi, Qbox code, qb@ll version, `https://github.com/LLNL/qball` (2017), Lawrence Livermore National Laboratory.

[38] A. Schleife, E. W. Draeger, V. M. Anisimov, A. A. Correa, and Y. Kanai, Quantum dynamics simulation of electrons in materials on high-performance computers, Comput. Sci. Eng. **16**, 54 (2014).

[39] E. Draeger, X. Andrade, J. Gunnels, A. Bhatele, A. Schleife, and A. Correa, Massively parallel first-principles simulation of electron dynamics in materials, J. Parallel Distrib. Comput. **106**, 205 (2017).

[40] R. M. Martin, L. Reining, and D. M. Ceperley, *Interacting Electrons: Theory and Computational Approaches* (Cambridge University Press, Cambridge, 2016).

[41] P. Ghosez, X. Gonze, and R. W. Godby, Long-wavelength behavior of the exchange-correlation kernel in the Kohn-Sham theory of periodic systems, Phys. Rev. B **56**, 12811 (1997).

[42] Y.-H. Kim and A. Görling, Exact Kohn-Sham exchange kernel for insulators and its long-wavelength behavior, Phys. Rev. B **66**, 035114 (2002).

[43] M. Friedrich, W. G. Schmidt, A. Schindlmayr, and S. Sanna, Optical properties of titanium-doped lithium niobate from time-dependent density-functional theory, Phys. Rev. Materials **1**, 034401 (2017).

[44] S. Sharma, J. K. Dewhurst, A. Sanna, and E. K. U. Gross, Bootstrap approximation for the exchange-correlation kernel of time-dependent density-functional theory, Phys. Rev. Lett. **107**, 186401 (2011).

[45] See Supplemental Material at http://... for the following details: (1) Construction of xc potentials from xc kernels. (2) Implementation of the scaled ALDA. (3) Real-time propagation with Qb@ll. (4) Optical response calculations with Yambo. (5) **k**-point sampling in TDDFT and BSE. (6) Time-dependent current densities in Si, H_2 chain, LiF, and $CsGeCl_3$. The Supplemental Material includes Refs. [60–72].

[46] J. R. Williams, N. Tancogne-Dejean, and C. A. Ullrich, Time-resolved exciton wave functions from time-dependent density-functional theory, J. Chem. Theory Comput. **17**, 1795 (2021).

[47] N. T. Maitra, I. Souza, and K. Burke, Current-density functional theory of the response of solids, Phys. Rev. B **68**, 045109 (2003).

[48] This is different in lower dimensions, where the head of the LRC kernel is ineffective and excitons are formed via local-field effect. Hence, in Ref. [46] the xc scalar potential is used.

[49] D. Sangalli *et al.*, Many-body perturbation theory calculations using the yambo code, J. Phys.: Condens. Matter **31**, 325902 (2019).

[50] P. Giannozzi *et al.*, Advanced capabilities for materials modelling with QUANTUM ESPRESSO, J. Phys.: Condens. Matter **29**, 465901 (2017).

[51] P. Lautenschlager, M. Garriga, S. Logothetidis, and M. Cardona, Interband critical points of GaAs and their temperature dependence, Phys. Rev. B **35**, 9174 (1987).

[52] A. Marini and R. Del Sole, Dynamical excitonic effects in

metals and semiconductors, Phys. Rev. Lett. **91**, 176402 (2003).

[53] D. Kammerlander, S. Botti, M. A. L. Marques, A. Marini, and C. Attaccalite, Speeding up the solution of the Bethe-Salpeter equation by a double-grid method and Wannier interpolation, Phys. Rev. B **86**, 125203 (2012).

[54] M. Grüning, D. Sangalli, and C. Attaccalite, Dielectrics in a time-dependent electric field: A real-time approach based on density-polarization functional theory, Phys. Rev. B **94**, 035149 (2016).

[55] D. M. Roessler and W. C. Walker, Optical constants of magnesium oxide and lithium fluoride in the far ultraviolet, J. Opt. Soc. Am. **57**, 835 (1967).

[56] F. Sottile, K. Karlsson, L. Reining, and F. Aryasetiawan, Macroscopic and microscopic components of exchange-correlation interactions, Phys. Rev. B **68**, 205112 (2003).

[57] S. Botti, A. Schindlmayr, R. Del Sole, and L. Reining, Time-dependent density functional theory for extended systems, Rep. Prog. Phys. **70**, 357 (2007).

[58] M. Mundt, S. Kümmel, R. van Leeuwen, and P.-G. Reinhard, Violation of the zero-force theorem in the time-dependent Krieger-Li-Iafrate approximation, Phys. Rev. A **75**, 050501(R) (2007).

[59] J. P. Perdew, K. Burke, and M. Ernzerhof, Generalized gradient approximation made simple, Phys. Rev. Lett. **77**, 3865 (1996), erratum: *ibid.* **78**, 1396 (1997).

[60] A. P. Gaiduk and V. N. Staroverov, How to tell when a model Kohn-Sham potential is not a functional derivative, J. Chem. Phys. **131**, 044107 (2009).

[61] L.-y. Huang and W. R. L. Lambrecht, Electronic band structure trends of perovskite halides: Beyond Pb and Sn to Ge and Si, Phys. Rev. B **93**, 195211 (2016).

[62] D. R. Hamann, Optimized norm-conserving Vanderbilt pseudopotentials, Phys. Rev. B **88**, 085117 (2013), erratum: *ibid.* **95**, 239906 (2017).

[63] M. van Setten, M. Giantomassi, E. Bousquet, M. Verstraete, D. Hamann, X. Gonze, and G.-M. Rignanese, The pseudodojo: Training and grading a 85 element optimized norm-conserving pseudopotential table, Comput. Phys. Commun. **226**, 39 (2018).

[64] A. Schleife, E. W. Draeger, Y. Kanai, and A. A. Correa, Plane-wave pseudopotential implementation of explicit integrators for time-dependent Kohn-Sham equations in large-scale simulations, J. Chem. Phys. **137**, 22A546 (2012).

[65] R. Haydock, The recursive solution of the Schrödinger equation, Comput. Phys. Commun. **20**, 11 (1980).

[66] L. X. Benedict and E. L. Shirley, Ab initio calculation of $\epsilon_2(\omega)$ including the electron-hole interaction: Application to GaN and CaF$_2$, Phys. Rev. B **59**, 5441 (1999).

[67] D. Varsano, A. Marini, and A. Rubio, Optical saturation driven by exciton confinement in molecular chains: A time-dependent density-functional theory approach, Phys. Rev. Lett. **101**, 133002 (2008).

[68] Z. H. Levine and D. C. Allan, Linear optical response in silicon and germanium including self-energy effects, Phys. Rev. Lett. **63**, 1719 (1989).

[69] X. Gonze and C. Lee, Dynamical matrices, Born effective charges, dielectric permittivity tensors, and interatomic force constants from density-functional perturbation theory, Phys. Rev. B **55**, 10355 (1997).

[70] H. J. Monkhorst and J. D. Pack, Special points for Brillouin-zone integrations, Phys. Rev. B **13**, 5188 (1976).

[71] D. Rocca, Y. Ping, R. Gebauer, and G. Galli, Solution of the Bethe-Salpeter equation without empty electronic states: Application to the absorption spectra of bulk systems, Phys. Rev. B **85**, 045116 (2012).

[72] S. Albrecht, L. Reining, G. Onida, V. Olevano, and R. Del Sole, Albrecht et al. reply:, Phys. Rev. Lett. **83**, 3971 (1999).